Seasonal Forecasting of North China Summer Rainfall Using a Statistical Downscaling Model

YAN GUO

State Key Laboratory of Earth Surface Processes and Resource Ecology, Beijing Normal University, and State Key Laboratory of Numerical Modeling for Atmospheric Sciences and Geophysical Fluid Dynamics, Institute of Atmospheric Physics, Chinese Academy of Sciences, Beijing, China

JIANPING LI

College of Global Change and Earth System Science, Beijing Normal University, and State Key Laboratory of Numerical Modeling for Atmospheric Sciences and Geophysical Fluid Dynamics, Institute of Atmospheric Physics, Chinese Academy of Sciences, Beijing, China

YUN LI

CSIRO Computational Informatics, CSIRO Climate Adaptation Flagship, Wembley, Western Australia, Australia

(Manuscript received 18 June 2013, in final form 12 February 2014)

ABSTRACT

A statistical downscaling model was developed with reanalysis data and applied to forecast northern China summer rainfall (NCSR) using the outputs of the real-time seasonal Climate Forecast System, version 2 (CFSv2). Large-scale climate signals in sea level pressure, 850-hPa meridional wind, and 500-hPa geopotential height as well as several well-known climate indices were considered as potential predictors. Through correlation analysis and stepwise screening, two ''optimal'' predictors (i.e., sea level pressure over the southwestern Indian Ocean and 850-hPa meridional wind over eastern China) were selected to fit the regression equation. Model reliability was validated with independent data during a test period (1991–2012), in which the simulated NCSR well represented the observed variability with a correlation coefficient of 0.59 and a root-mean-square error of 18.6%. The statistical downscaling model was applied to forecast NCSR for a 22-yr period (1991–2012) using forecast predictors from the CFSv2 with lead times from 1 to 6 months. The results showed much better forecast skills than that directly from the CFSv2 for all lead months, except the 3-month-lead example. The biggest improvement occurred in the 1-month-lead forecast, in which the hit rate increased to 77.3% from 45.5% in the CFSv2 forecast. In the forecast of rainfall at 15 stations, the statistical downscaling model also showed superior capability when compared with the CFSv2, with forecast skill being improved at 73% of stations. In particular, 13 of 15 stations obtained a hit rate exceeding 55%.

1. Introduction

As one of the particular focuses of the World Climate Research Programme's Climate Variability and Predictability (CLIVAR) project, seasonal forecasting is of great significance. Although state-of-the-art climate models have been improved significantly and have been verified to be useful tools for seasonal forecasting, their forecast skill for precipitation, especially for Asian summer monsoon precipitation, remains limited (Wu et al. 2009; Lee et al. 2011). North China, with its enormous population and rapid social and economic development, is located at the northern boundary of the East Asia subtropical monsoon region and receives the bulk of its annual rainfall during boreal summer, primarily falling in July and August. The north China summer rainfall (NCSR) variability is influenced by both the mid- to high-latitude circulation patterns and the East Asian summer monsoon system, of which the location and magnitude of the

Corresponding author address: Dr. Jianping Li, State Key Laboratory of Numerical Modeling for Atmospheric Sciences and Geophysical Fluid Dynamics, Institute of Atmospheric Physics, Chinese Academy of Sciences, Beijing 100029, China.
E-mail: ljp@lasg.iap.ac.cn

DOI: 10.1175/JAMC-D-13-0207.1

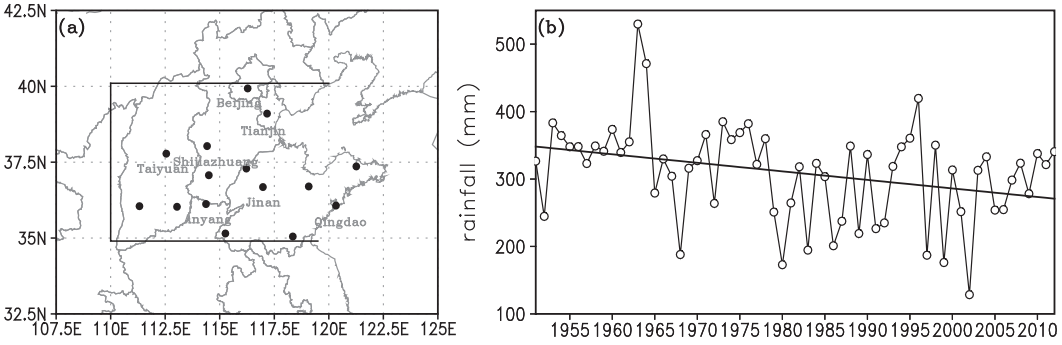

FIG. 1. (a) Locations of rain gauge stations in the north China region (35°–40°N, 110°–122°E). (b) Time series of north China July–August rainfall and its linear trend over 1951–2012.

western North Pacific subtropical high (WNPSH) play the most important role (Zhao and Song 1999; Huang et al. 2008). As such, NCSR has complicated variability on both interannual and interdecadal scales (Huang et al. 1999; Lu 2003; Fu et al. 2009). North China is one of the regions frequently plagued by severe droughts and floods (Wu et al. 2012a,b). Seasonal forecasting of NCSR is an important issue that is directly related disaster prevention and mitigation. However, improving the forecast skill for NCSR has long been a challenge for Chinese meteorologists (Peng et al. 2006; Fan et al. 2009; Wei and Huang 2010).

General circulation models (GCMs) are generally good at simulating large-scale climate variables (e.g., mean sea level pressure); they are unable to capture subgrid processes, however, and fail to simulate rainfall on regional and subregional scales (Hewitson and Crane 2006). Because of this limitation, a statistical downscaling technique has emerged and has experienced rapid improvement in the past few decades. This technique describes the regional climate via a statistical relationship linked to large-scale climate signals that can be well simulated by GCMs (Zorita and von Storch 1999; Fowler et al. 2007). The statistical downscaling technique has been widely applied to forecasting and predicting regional climate (Charles et al. 1999; Benestad 2002; Landman and Goddard 2002; Oshima et al. 2002; Feddersen and Andersen 2005; Chu et al. 2008; Zhu et al. 2008; Li and Smith 2009; Juneng et al. 2010; Chen et al. 2012; Guo et al. 2012; Liu and Fan 2012). With the demand for improving the operational forecast skill for NCSR in mind, in this paper we intend to develop a statistical downscaling model of NCSR and apply it to produce forecasts with lead times extending to 6 month, using the National Centers for Environmental Prediction's (NCEP) Climate Forecast System, version 2 (CFSv2).

The remainder of this paper is structured as follows. Sections 2 and 3 introduce the data and the statistical downscaling scheme. The performance of the statistical model is provided in section 4. In section 5, the statistical model is applied to forecast NCSR and rainfall at 15 individual stations for a 22-yr period (1991–2012) using the CFSv2. A summary and discussion are presented in section 6.

2. Data

Observed precipitation data were obtained from China's 160-station monthly rainfall dataset provided by the China Meteorological Administration (CMA) for the period 1951–2012. The north China region was defined as a box bounded by 35°–40°N, 110°–122°E. The averaged summer (July and August) rainfall totals at 15 uniformly spread stations in north China (Fig. 1a) were generated as the NCSR time series. As shown in Fig. 1b, a significant decreasing trend exists in NCSR during the past 62 yr that contains remarkable interannual and decadal variations.

Reanalysis data were used to establish the statistical downscaling model. Sea level pressure (SLP), 850-hPa meridional wind (V_{850}), and 500-hPa geopotential height (GHT_{500}) were used as potential predictor variables that represent large-scale circulation anomalies as the basis for precipitation. Several well-known large-scale climate indices were also used as potential predictors. The Niño-3.4 index was used to represent the ENSO phenomenon (available online at http://www.cpc.noaa.gov/data/indices/). The southern annular mode index (SAMI) is defined as the difference in normalized monthly zonal-mean SLP between 40° and 70°S (Nan and Li 2003) and is available online (at http://web.lasg.ac.cn/staff/ljp/dataset.html/). The Indian Ocean dipole index (IODI) was calculated following the definition proposed by Saji et al. (1999). The index of the latitude location of the WNPSH ridge was calculated over 110°–150°E using the 500-hPa geopotential height following the definition provided by the CMA. The East Asian summer monsoon index (EASMI) is defined as the area-averaged dynamical normalized seasonality at 850 hPa within the domain 10°–40°N, 110°–140°E (Li and

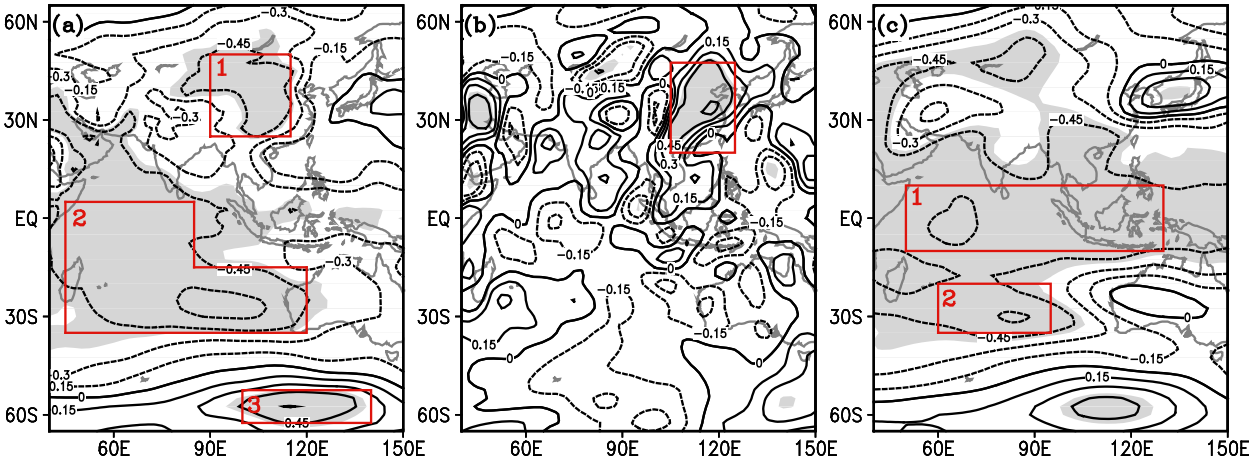

FIG. 2. Correlation of detrended time series between NCSR and (a) sea level pressure, (b) 850-hPa meridional wind, and (c) 500-hPa geopotential height for the period 1951–90. The shading indicates statistical significance at the 0.01 level. Red rectangles indicate areas having high correlation coefficients.

Zeng 2002, 2003; Li et al. 2010) and is available online (http://web.lasg.ac.cn/staff/ljp/dataset.html). The atmospheric data were obtained from the NCEP–National Center for Atmospheric Research (NCAR) reanalysis dataset on a 2.5° × 2.5° grid, and the sea surface temperature (SST) data were obtained from the Hadley Centre SST dataset on a 1° × 1° grid.

To verify the forecast capability of the statistical downscaling model, CFSv2 monthly data covering the 31-yr period of 1982–2012 from the retrospective forecast experiment (1982–2010) and the operational forecast (2011–12) were employed (Saha et al. 2012). CFSv2 is the second version of fully coupled dynamical seasonal prediction systems developed at the Environmental Modeling Center at NCEP and became operational in 2011. It initiated every month with an integration period of 9 months. In every forecast, 24 members were designed with different initial conditions (different starting times). As a matter of convenience, only the ensemble mean, which was calculated as the simple average of 24 members (equal weight), was used in this study.

3. Statistical downscaling scheme

A multilinear regression approach is used to develop the statistical downscaling model. Correlation analysis is first used to identify potential predictors on a global scale, from which the predictors are further selected with a cross-validation-based stepwise regression method to fit the final regression equation.

Given the predictor variable, we calculate the correlation map between the predictor variable field and the predictand. To avoid any relationship that may arise from trends in the predictand as well as the predictor variable, all data are detrended before calculating the correlation coefficient. Any large-scale domain with a significant correlation coefficient is identified, and the corresponding area-weighted average value is calculated into an index as a potential predictor. A running correlation between the potential predictor and the predictand is then conducted to ensure a stable and robust correlated relationship. Not every potential predictor is necessary in fitting the final regression equation. A stepwise regression method nested with leave-five-out cross validation (Wu et al. 2009) is utilized to select the optimal predictors from the original potential predictors. Details of this statistical downscaling scheme are available in the study by Guo et al. (2012).

In addition, an independent test was carried by dividing the whole dataset into a training period (1951–90) and an independent test period (1991–2012). To quantify the uncertainty degree of the prediction, a bootstrap resampling approach (Stine 1985) was employed to obtain the 95% confidence interval from the spread of 1000 bootstrap samples with random replacement.

4. Statistical downscaling model of NCSR

Figure 2 shows the correlation maps of the detrended time series between NCSR and three circulation fields during the training period (1951–90). Six domains having significant correlation coefficients at the 0.01 level are identified, and the area-weighted average values over these six domains are calculated into indices, labeled as $SLP_{(1)–(3)}$, V_{850}, and $GHT_{(1)–(2)}$. All six indices are significantly correlated with NCSR (Table 1). In addition, several well-known large-scale climate indices, such as the Niño-3.4 index, SAMI, EASMI, the index of the latitude

TABLE 1. Definitions of potential predictors and their correlation coefficients with NCSR for the period 1951–90.

Variable	Level	Area	Label	Correlation	
				Raw	Detrended
Sea level pressure	Surface	25°–50°N, 90°–115°E	$SLP_{(1)}$	−0.6	−0.52
Sea level pressure	Surface	35°–15°S, 45°–120°E 15°S–5°N, 45°–85°E	$SLP_{(2)}$	−0.72	−0.67
Sea level pressure	Surface	62.5°–52.5°S, 100°–140°E	$SLP_{(3)}$	0.64	0.58
Meridional wind	850 hPa	20°–47.5°N, 105°–125°E	V_{850}	0.63	0.61
Geopotential height	500 hPa	10°S–10°N, 50°–130°E	$GHT_{500(1)}$	−0.64	−0.57
Geopotential height	500 hPa	35°–20°S, 60°–95°E	$GHT_{500(2)}$	−0.69	−0.65

location of the WNPSH ridge, and IODI, which have impacts on global climate, are also taken into account as potential predictors.

To examine the stability of the correlation coefficients between the potential predictors and NCSR, a running correlation with a 21-yr sliding window is conducted on the detrended time series (Fig. 3). It appears that five indices of $SLP_{(2)–(3)}$, V_{850}, and $GHT_{500(1)–(2)}$ have stable significant correlations with NCSR (at the 0.05 level), while the rest do not have stable significant correlations with NCSR. Therefore, the indices of $SLP_{(2)–(3)}$, V_{850}, and $GHT_{500(1)–(2)}$ are retained and used with the stepwise screening procedure, while the others are excluded.

In the stepwise screening procedure, the potential predictors for $SLP_{(2)}$ and V_{850} are successively selected into the regression equation because they produce minimum root-mean-square errors (RMSEs) in cross validation of 52.13 mm in step 1 and 50.11 mm in step 2, respectively. No further decrease in RMSE is found by adding additional predictors into the regression equation. Thus, $SLP_{(2)}$ and V_{850} are selected, and the regression equation is finally fitted in the form given by

$$Y(t) = 320.5 - 38.8\mathrm{SLP}_{(2)}(t) + 19.6V_{850}(t), \quad (1)$$

where $Y(t)$ is NCSR at year t ($t = 1, \ldots, 40$) over the 1951–90 period and $\mathrm{SLP}_{(2)}(t)$ and $V_{850}(t)$ are the tth observed values of the normalized indices of the SLP averaged over the southwestern Indian Ocean (IO) and the 850-hPa meridional wind averaged over eastern China, respectively. Note that the regression coefficients of $SLP_{(2)}$ and V_{850} are both found to be significantly different from 0 at the 0.05 level by using the Student's t test.

The empirical relationship derived between the predictors and the predictand should be physically interpretable. In this regard, we explore the associated circulations that link the predictors $SLP_{(2)}$ and V_{850} with the NCSR.

The first predictor $SLP_{(2)}$ represents the SLP over the southwestern IO and is associated with the ENSO-related SST pattern (Fig. 4a). The correlation coefficient between $SLP_{(2)}$ and the Niño-3.4 index is 0.47 (0.49 for the detrended time series), significant at the 0.05 level. From the partial correlation map between $SLP_{(2)}$ and the surface air temperature field after linearly

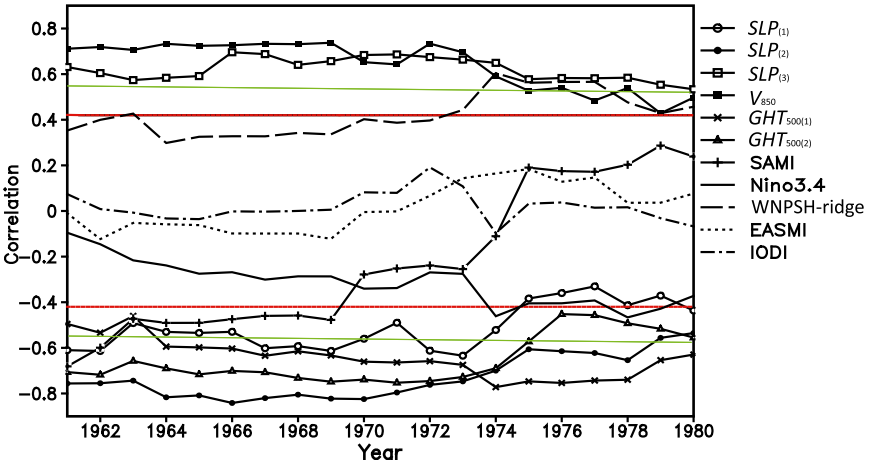

FIG. 3. The 21-yr sliding-window correlations of NCSR with six potential predictors—$SLP_{(1)–(3)}$, V_{850}, and $GHT_{500(1)–(2)}$—and several large-scale climate indices for the period 1951–90. Red (green) horizontal lines denote significance at the 0.05 (0.01) level. All trends associated with the sliding window have been removed.

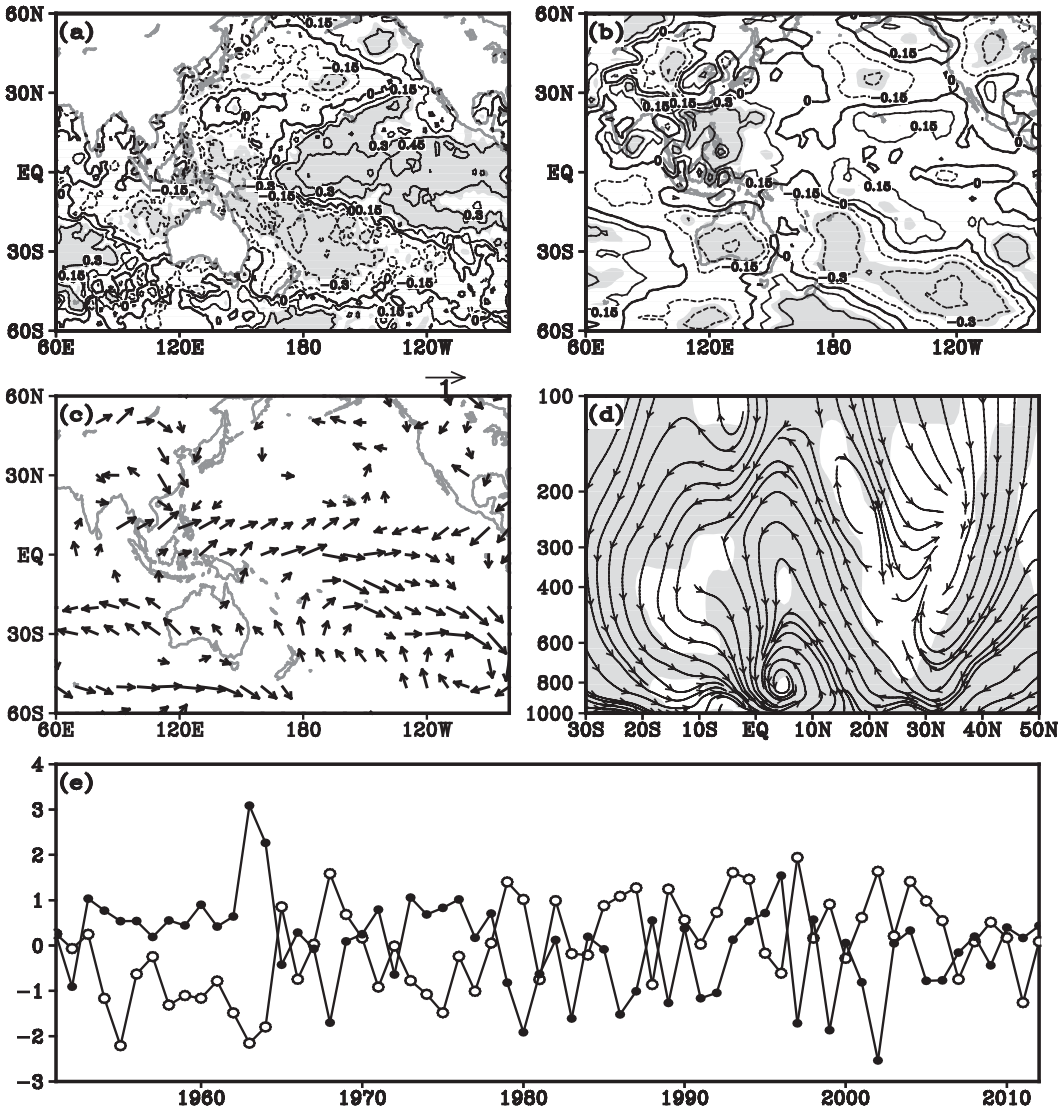

FIG. 4. Correlation of detrended time series between $SLP_{(2)}$ and (a) sea surface temperature, (b) surface air temperature after linearly removing the Niño-3.4 index, (c) surface winds, and (d) meridional circulation along a latitude–pressure cross section averaged over 100°–140°E. Significance at the 0.05 level is denoted by shading in (a), (b), and (d) and with vectors in (c), plotted only if the correlation coefficients for both the u and v directions are significant. (e) Normalized time series of $SLP_{(2)}$ (open circles) and NCSR (filled circles).

removing the Niño-3.4 index (Fig. 4b), the surface air temperature over the northwestern Pacific Ocean (western Pacific warm pool) exhibits significant correlation, indicating that the SLP increase over the southwestern IO is possibly relevant to the warming over the western Pacific warm pool as well as the eastern tropical Pacific.

Figure 4c shows the correlation of the detrended $SLP_{(2)}$ with the surface winds. It appears that, corresponding to the SLP increase over the southwestern IO, the low-level northward cross-equatorial current at 70°–100°E is intensified. The current turns to a southwesterly direction after crossing the equator and encountering the northeast trade winds, enhancing the low-level convergence in the intertropical convergence zone over the southern South China Sea and the Philippine Sea. Anomalous low-level convergence drives a positive meridional circulation anomaly in the north, one branch of which, the surface northerly anomaly on the eastern Asian coast, inhibits the northward expansion of the warm and wet monsoon flows. Meanwhile, the descending branch of the positive meridional circulation is approximately distributed at 40°N, resulting in north China being under the influence of downdrafts (Fig. 4d). Under the conditions of deficient moisture and an

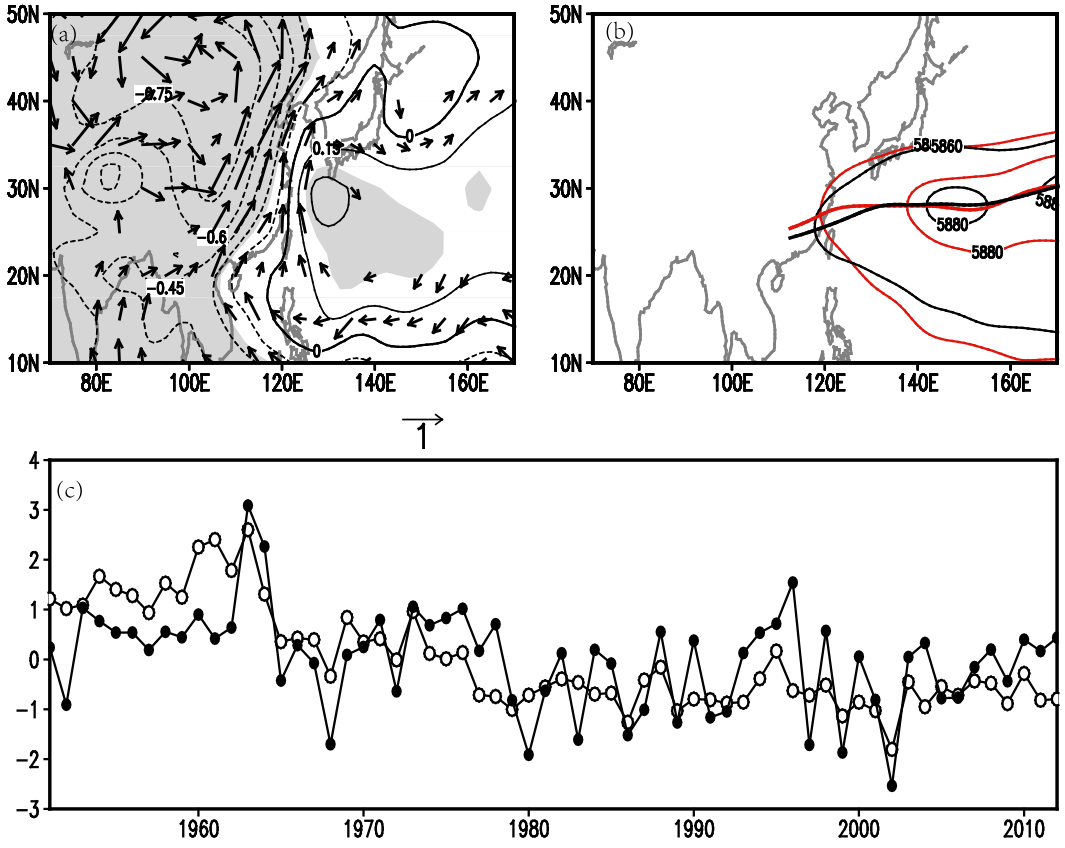

FIG. 5. (a),(c) As in Fig. 4, but for V_{850} with horizontal winds and geopotential height at the 850-hPa level. (b) Composite of the 500-hPa geopotential height and the ridge in the strong (red) and weak (black) V_{850} cases (anomalies exceeding 1 standard deviation in the detrended time series).

anomalous downward airstream, precipitation is suppressed over north China. Figure 4e shows the normalized time series of $SLP_{(2)}$ and NCSR. It is obvious that a negatively correlated relationship indeed exists between these two time series. In brief, $SLP_{(2)}$ is negatively associated with NCSR via a meridional circulation that NCSR is suppressed (enhanced) when $SLP_{(2)}$ is a positive (negative) anomaly.

The second predictor V_{850} represents the meridional wind over eastern China. Figure 5a shows a correlation map of the detrended time series between V_{850} and the horizontal winds and geopotential height at 850 hPa. Corresponding to the positive V_{850} anomaly (i.e., the southerly anomaly), an anomalous cyclone appears in eastern Asia, and an anomalous anticyclone appears in the northwestern Pacific. The composite of 500-hPa geopotential height and the WNPSH ridge in the strong and weak V_{850} cases (anomalies exceeding one standard deviation in the detrended time series) are shown in Fig. 5b. It is obvious that a northward shift of the western part of the WNPSH concurrently occurs with the anomalous strong V_{850}. The correlation coefficient between the index of latitude location of the WNPSH ridge and V_{850} is 0.29, which is significant at the 0.05 level. This suggests that the latitude location of the WNPSH ridge may affect the meridional wind over eastern China that modulates the water vapor transport from the South China Sea and the western Pacific to north China. If V_{850} is a positive anomaly, more warm and humid air is transported to the north, resulting in an anomalous wet summer in north China and vice versa. This result is consistent with the findings reported upon in the study of Li et al. (2012). Figure 5c shows the normalized time series of V_{850} and NCSR, revealing the generally consistent variation.

Figure 6a compares the observed and simulated rainfall amounts during both the training period (1951–90) and the independent test period (1991–2012). The uncertainty in terms of 95% confidence intervals is indicated with blue dashed lines. In general, the statistical model provides a relatively accurate representation of the observations. The performance evident in the training period is mostly maintained during the subsequent verification period. The correlation coefficient and RMSE between the simulated and observed rainfall amounts are

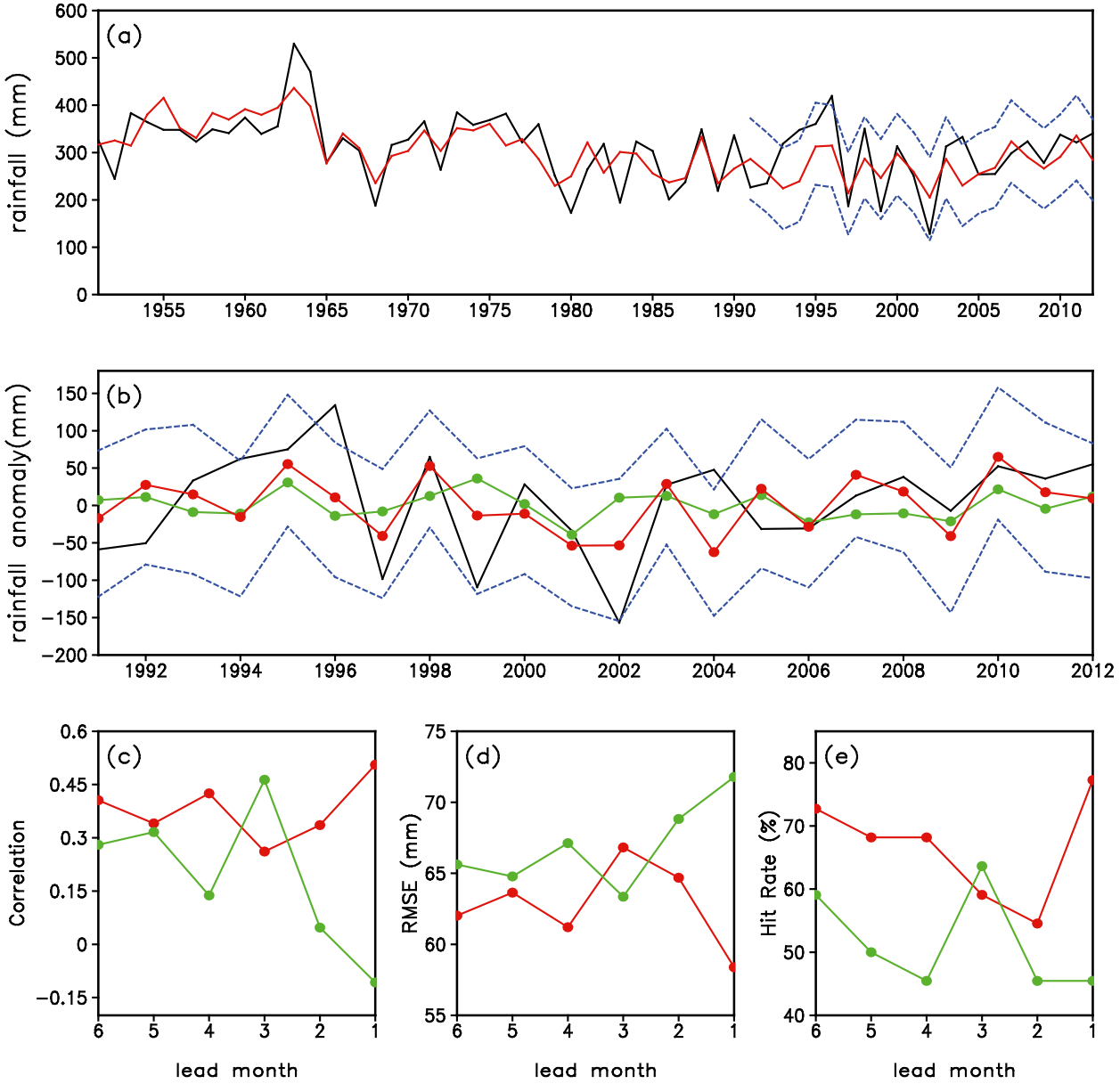

FIG. 6. (a) Observed (black) and simulated (red) NCSR with the statistical downscaling model during the training period (1951–90) and independent test period (1991–2012). (b) Observed (black) and 1-month-lead forecast NCSR anomalies from the CFSv2 (green) and the statistical downscaling model (red) during 1991–2012. Blue dashed lines indicate 95% confidence intervals. The forecast skill for NCSR with lead times based on the statistical downscaling model (red) and the CFSv2 (green) as measured by (c) correlation coefficient, (d) RMSE, and (e) hit rate, the ratio of years in which the anomaly sign is correctly forecast to the total number of years.

0.76 and 46.6 mm (15.1% of the climatology) during the training period and 0.59 and 57.5 mm (18.6% of the climatology) during the independent test period.

5. Application of the statistical downscaling model to forecasting NCSR

To test the forecast capability of NCSR using the statistical downscaling model in Eq. (1), a forecast experiment for a 22-yr period (1991–2012) was performed using the predictors forecast ahead by the CFSv2. To reduce the systematic bias in CFSv2, such as climatology drift, we first adjusted the CFSv2 output by correcting the climatology bias. On account of the limited extension of the CFSv2 retrospective forecast data (starting from 1982), the climatology bias was calculated based on the period starting from 1982 to the prior year.

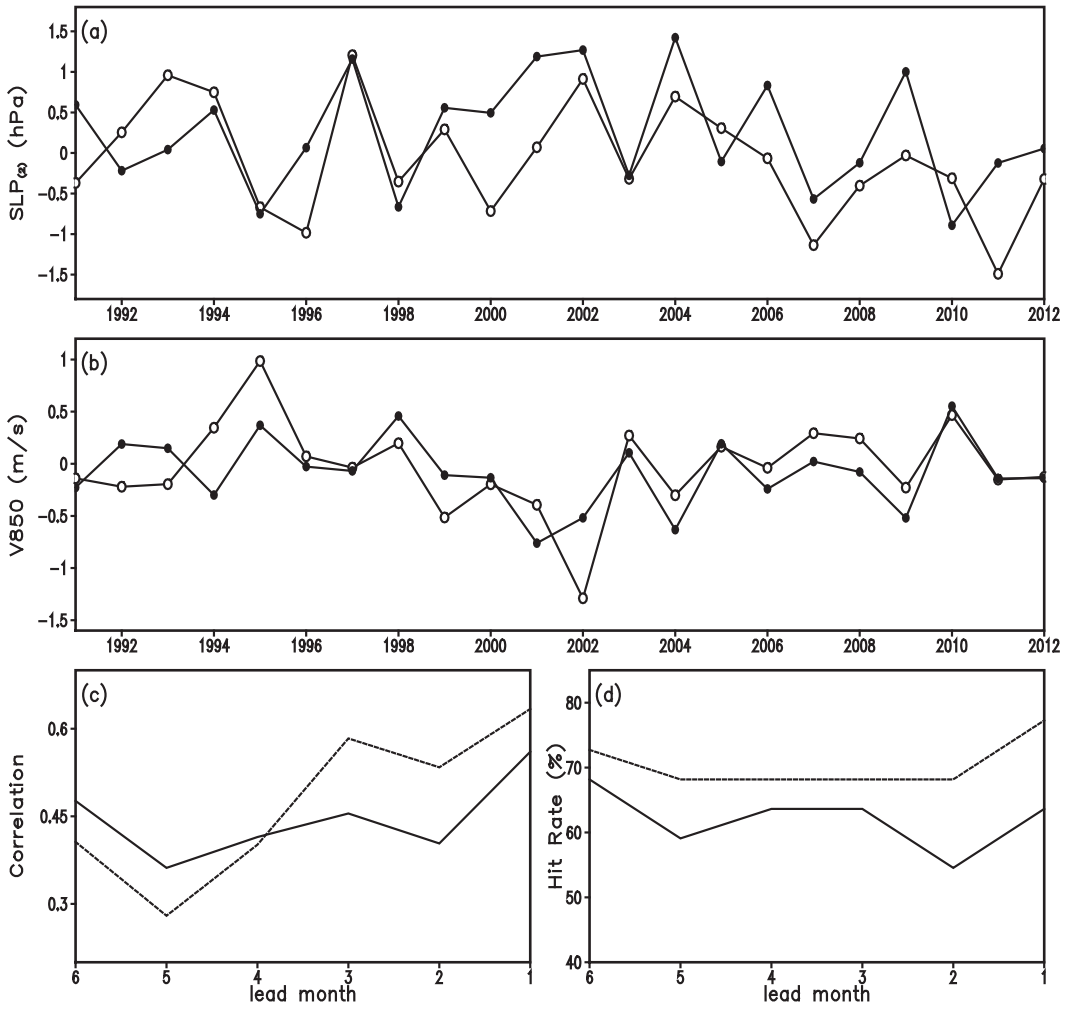

FIG. 7. Observed (open circles) and 1-month-lead forecast (filled circles) anomalies of predictors (a) $SLP_{(2)}$ and (b) V_{850} by the CFSv2 during 1991–2012. (c),(d) As in Figs. 6c and 6e, respectively, but for predictors $SLP_{(2)}$ (solid) and V_{850} (dashed) with lead times based on the CFSv2.

Figure 6b shows the 1-month-lead NCSR anomaly forecast by both the CFSv2 and the statistical downscaling model. The uncertainty in terms of 95% confidence intervals is indicated by blue dashed lines. It appears that CFSv2 can barely forecast the interannual variability, since it only correctly forecasts the sign of the rainfall anomaly in 10 of the 22 yr, a hit rate (i.e., the ratio of years in which the anomaly sign is correctly forecast to the total years) of 45.5%. In contrast, the statistical downscaling model has considerably improved the forecast with a hit rate of 77.3% and a correlation coefficient of 0.51, while the RMSE is reduced from 71.8 mm in the CFSv2 forecast to 58.4 mm in the statistical downscaled results. Figures 7a and 7b show the 1-month-lead forecast anomalies of two predictors of $SLP_{(2)}$ and V_{850} by the CFSv2. It is clear that CFSv2 is fairly good at forecasting the two predictors with correlation coefficients of 0.56 and 0.63 and hit rates of 63.6% and 77.2%, respectively.

In addition to the 1-month-lead forecast, additional forecasts with lead times extending up to 6 months were produced. Figures 6c–e show the *skill* of the forecasts with lead times from 1 to 6 months based on the CFSv2 and the statistical downscaling model, respectively, measured in terms of the correlation coefficient, RMSE, and hit rate. In comparison with the CFSv2, the statistical downscaling model shows much better skill in all forecasts except the 3-month-lead case. In the statistical downscaled results, the 1-month-lead forecast has the highest skill. It is noteworthy that the forecast skill does not monotonously decrease as lead time increases. Two forecasts with lead times at 2 and 3 months show relatively poor performance, which is primarily due to inferior forecasting of the $SLP_{(2)}$ by the CFSv2 (Figs. 7c,d).

TABLE 2. The metrics of 1-month-lead forecast summer rainfall at 15 stations during the 22-yr period (1991–2012) using the statistical downscaling model and the CFSv2 (values in parentheses). Correlation and RMSE are the correlation coefficient and root-mean-square error between the observed and forecast rainfall amounts during 1991–2012. Hit rate is the ratio of years in which the anomaly sign is correctly forecast to the total number of years.

Station	Correlation	RMSE (mm)	Hit rate (%)	Station	Correlation	RMSE (mm)	Hit rate (%)
Anyang	0.22 (0.05)	107 (104)	59 (59)	Qingdao	0.27 (−0.06)	131 (139)	68 (55)
Beijing	0.16 (−0.18)	135 (141)	68 (41)	Shijiazhuang	0.15 (−0.05)	168 (172)	59 (50)
Changzhi	0.47 (0.41)	80 (83)	64 (55)	Taiyuan	0.20 (0.30)	76 (74)	59 (64)
Dezhou	0.48 (0.06)	103 (118)	73 (59)	Tianjin	0.06 (0.15)	110 (100)	50 (59)
Heze	0.25 (0.12)	123 (126)	55 (59)	Weifang	−0.25 (−0.04)	110 (113)	36 (45)
Jinan	0.38 (0.18)	120 (124)	68 (50)	Xingtai	0.30 (−0.14)	113 (123)	59 (36)
Linfen	0.50 (0.26)	67 (74)	68 (59)	Yantai	0.45 (0.23)	112 (121)	73 (64)
Linyi	0.35 (0.02)	127 (139)	68 (59)				

To explore the ability of the statistical downscaling model to forecast rainfall at individual stations, a separate model was derived using the observed rainfall data at each of 15 stations and the predictors of $SLP_{(2)}$ and V_{850} over the training period 1951–90. By substituting the 1-month-lead forecast values of $SLP_{(2)}$ and V_{850} from the CFSv2 into each fitted statistical equation, one may obtain the forecast rainfall values covering a 22-yr period (1991–2012) for each individual station. Table 2 compares the forecast skill between the statistical downscaling model and the CFSv2 at each station measured in terms of the correlation coefficient, RMSE, and hit rate. It is obvious that combining the statistical downscaling model and the predictors forecast by the CFSv2 generally provides a better degree of skill than the directly rainfall forecasts from the CFSv2. By using the statistical downscaling model, 13 of 15 stations (87%) have hit rates exceeding 55%, 47% of the stations have hit rates exceeding 65%, and 13% of the stations have hit rates exceeding 70%. This outperforms the CFSv2 forecasts in which 60% of the stations have hit rates exceeding 55%, and none of the stations exceeds 65%. With the exception of four stations (Anyang, Tianjin, Taiyuan, and Weifang), the forecast skills at the other 11 stations are improved according to all of the three measurements. The most significant improvement appears at the Xingtai, Beijing, and Dezhou stations, where the hit rates increase by 23%, 27%, and 14%, and the correlation coefficients increase by 0.44, 0.36, and 0.42, respectively.

6. Summary and discussion

In this study, a statistical downscaling model of NCSR was developed with reanalysis data and applied to forecasting NCSR over a 22-yr period using the CFSv2. The key findings of this study are summarized as follows.

Through correlation analysis and a stepwise screening procedure, two predictors (SLP averaged over the southwestern IO and 850-hPa meridional winds over eastern China) were selected to fit the multilinear regression equation, which was referred to as a statistical downscaling model of NCSR. It was further shown that the SLP over southwestern IO was negatively associated with NCSR via cross-equatorial stream-induced anomalous meridional circulation, while the meridional wind over eastern China was positively relevant to NCSR through modulating the northward moisture transport. The statistically downscaled results provided a good representation of the observed NCSR, with a correlation coefficient and an RMSE of 0.76 and 46.6 mm (15.1%) during the training period and 0.59 and 57.5 mm (18.6%) during the independent test period, respectively. The statistical downscaling model was then applied to forecast NCSR for a 22-yr period (1991–2012) using forecast predictors from the CFSv2 with lead times from 1 to 6 months. The results showed much better forecast skills than that directly from the CFSv2 for all lead months, except the 3-month-lead example. The biggest improvement occurred in the 1-month-lead forecast, in which the hit rate increased to 77.3% from 45.5% in the CFSv2 forecast. In the forecast rainfall at 15 stations, the statistical downscaling model also showed superior capability relative to the CFSv2, with the forecast skill showing improvement at 73% of the stations. In particular, 87% of the stations had the hit rates exceeding 55%, 47% of the stations exceeded 65%, and 13% of the stations exceeded 70%.

Bear in mind that the statistical downscaling model was developed using historical reanalysis data, following the perfect prognosis method rather than the model output statistics method. Thus, a reliable forecast of the predictors is necessary. As shown in Figs. 6c–e, the forecasts with lead times at 2 and 3 had inferior skill, which primarily resulted from the relatively poor forecasts of the $SLP_{(2)}$ by the CFSv2 (Figs. 7c,d). These two forecasts in CFSv2 started at the beginning of May and April, respectively; thus, the relatively low skill in the $SLP_{(2)}$

forecasts is likely relevant to the spring prediction barrier in CFSv2, which warrants further investigations.

As shown above, the statistical downscaling model significantly improved the forecast of NCSR particularly in 1-month-lead forecasts, and there is still room for further improvement. In this study, we only considered circulation variables as predictors. The final results demonstrated that the selected circulation predictors captured most of the variability in NCSR; however, it does not mean that other climate variables are not necessary, especially humidity-related variables. In addition, as Lu (2003) reported, the NCSR variability has multiscale features, and variations on different time scales are associated with different circulation patterns. It is appropriate to calibrate distinct empirical equations to forecast the individual variability components. The superiority of the time-scale decomposition approach in the statistical downscaling of NCSR has been demonstrated by Guo et al. (2012).

CFSv2 forecast NCSR 3 months ahead reasonably well, but its performance in forecasts with lead times at 1 and 2 months was unexpectedly poor (Figs. 6c–e). Meanwhile, the associated large-scale circulation, the low-level meridional wind in eastern China (V_{850}), was well forecast in all three cases (Figs. 7c,d). This indicated that CFSv2's forecast skill for NCSR was not limited by its forecasts for the low-level meridional wind, and some other factors may be the source of the forecast uncertainty, like insufficient resolution and imperfect parameterization.

This study focused on regional average summer rainfall over north China, although we conducted forecasts of rainfall at individual stations within north China as well. The predictors employed to regress the rainfall at 15 stations were exactly the same as those for NCSR. If we were to identify particular predictors for individual stations and develop an empirical relationship, the forecast skill, especially at stations like Weifang, which has a distinctive rainfall variability among all the stations, would be further improved. In addition, the diminished forecast skill at the Tianjin and Taiyuan stations possibly revealed the limitations of statistical downscaling at sites affected by large-scale climate factors rather than at sites primarily influenced by mesoscale and microscale processes; as are the sites in mountainous (Taiyuan) or coastal (Tianjin) areas. Additional reasons for the poor performance at these stations deserve deeper investigation in the future.

Finally, the statistically downscaled results are constrained by the quality of the predictors [e.g., $SLP_{(2)}$] used in the forecasts by the CFSv2. In this case, a better and greater consensus about the forecast predictors from different seasonal forecast climate models may lead to an improved consensus of rainfall forecasts using downscaling techniques. Future work will investigate the application of these techniques to an ensemble of seasonal forecast climate model results.

Acknowledgments. We thank three anonymous reviewers for their comments and suggestions. This study was jointly supported by the 973 Program (2010CB950400), NSFC Key Project (41030961) and the Australia-China Bilateral Climate Change Partnerships Program of the Australian Department of Climate Change. Yun Li was also supported by a Western Australian state government Indian Ocean Climate Initiative Project.

REFERENCES

Benestad, R. E., 2002: Empirically downscaled multimodel ensemble temperature and precipitation scenarios for Norway. *J. Climate,* **15,** 3008–3027, doi:10.1175/1520-0442(2002)015<3008:EDMETA>2.0.CO;2.

Charles, S. P., B. C. Bates, and J. P. Hughes, 1999: A spatiotemporal model for downscaling precipitation occurrence and amounts. *J. Geophys. Res.,* **104,** 31 657–31 669, doi:10.1029/1999JD900119.

Chen, H., J. Sun, and H. Wang, 2012: A statistical downscaling model for forecasting summer rainfall in China from DEMETER hindcast datasets. *Wea. Forecasting,* **27,** 608–628, doi:10.1175/WAF-D-11-00079.1.

Chu, J.-L., H. Kang, C.-Y. Tam, C.-K. Park, and C.-T. Chen, 2008: Seasonal forecast for local precipitation over northern Taiwan using statistical downscaling. *J. Geophys. Res.,* **113,** D12118, doi:10.1029/2007JD009424.

Fan, K., M. Lin, and Y. Gao, 2009: Forecasting the summer rainfall in North China using the year-to-year increment approach. *Sci. China,* **52D,** 532–539, doi:10.1007/s11430-009-0040-0.

Feddersen, H., and U. Andersen, 2005: A method for statistical downscaling of seasonal ensemble predictions. *Tellus,* **57A,** 398–408, doi:10.1111/j.1600-0870.2005.00102.x.

Fowler, H. J., S. Blenkinsop, and C. Tebaldi, 2007: Linking climate change modelling to impacts studies: Recent advances in downscaling techniques for hydrological modelling. *Int. J. Climatol.,* **27,** 1547–1578, doi:10.1002/joc.1556.

Fu, G., S. P. Charles, J. Yu, and C. Liu, 2009: Decadal climatic variability, trends, and future scenarios for the north China plain. *J. Climate,* **22,** 2111–2123, doi:10.1175/2008JCLI2605.1.

Guo, Y., J. P. Li, and Y. Li, 2012: A time-scale decomposition approach to statistically downscale summer rainfall over north China. *J. Climate,* **25,** 572–591, doi:10.1175/JCLI-D-11-00014.1.

Hewitson, B. C., and R. G. Crane, 2006: Consensus between GCM climate change projections with empirical downscaling: Precipitation downscaling over South Africa. *Int. J. Climatol.,* **26,** 1315–1337, doi:10.1002/joc.1314.

Huang, R. H., G. Huang, and B. H. Ren, 1999: Advances and problems needed for further investigation in the studies of the East Asian summer monsoon (in Chinese). *Chin. J. Atmos. Sci.,* **23,** 129–141.

——, L. Gu, J. L. Chen, and G. Huang, 2008: Recent progresses in studies of the temporal-spatial variations of the East Asian monsoon system and their impacts on climate anomalies in China (in Chinese). *Chin. J. Atmos. Sci.,* **32,** 691–719.

Juneng, L., F. T. Tangang, H. Kang, W.-J. Lee, and Y. K. Seng, 2010: Statistical downscaling forecasts for winter monsoon precipitation in Malaysia using multimodel output variables. *J. Climate,* **23,** 17–27, doi:10.1175/2009JCLI2873.1.

Landman, W. A., and L. Goddard, 2002: Statistical recalibration of GCM forecasts over southern Africa using model output statistics. *J. Climate,* **15,** 2038–2055, doi:10.1175/1520-0442(2002)015<2038:SROGFO>2.0.CO;2.

Lee, S.-S., J.-Y. Lee, K.-J. Ha, B. Wang, and J. K. E. Schemm, 2011: Deficiencies and possibilities for long-lead coupled climate prediction of the western North Pacific–East Asian summer monsoon. *Climate Dyn.,* **36,** 1173–1188, doi:10.1007/s00382-010-0832-0.

Li, J. P., and Q. C. Zeng, 2002: A unified monsoon index. *Geophys. Res. Lett.,* **29**, doi:10.1029/2001GL013874.

——, and ——, 2003: A new monsoon index and the geographical distribution of the global monsoons. *Adv. Atmos. Sci.,* **20,** 299–302, doi:10.1007/s00376-003-0016-5.

——, Z. Wu, Z. Jiang, and J. He, 2010: Can global warming strengthen the East Asian summer monsoon? *J. Climate,* **23,** 6696–6705, doi:10.1175/2010JCLI3434.1.

Li, Y., and I. Smith, 2009: A statistical downscaling model for southern Australia winter rainfall. *J. Climate,* **22,** 1142–1158, doi:10.1175/2008JCLI2160.1.

——, J. P. Li, and J. Feng, 2012: A teleconnection between the reduction of rainfall in southwest Western Australia and north China. *J. Climate,* **25,** 8444–8461, doi:10.1175/JCLI-D-11-00613.1.

Liu, Y., and K. Fan, 2012: Prediction of spring precipitation in China using a downscaling approach. *Meteor. Atmos. Phys.,* **118,** 79–93, doi:10.1007/s00703-012-0202-z.

Lu, R., 2003: Linear relationship between the interdecadal and interannual variabilities of north China rainfall in rainy season. *Chin. Sci. Bull.,* **48,** 1040–1044.

Nan, S., and J. P. Li, 2003: The relationship between the summer precipitation in the Yangtze River valley and the boreal spring Southern Hemisphere annular mode. *Geophys. Res. Lett.,* **30,** 2266, doi:10.1029/2003GL018381.

Oshima, N., H. Kato, and S. Kadokura, 2002: An application of statistical downscaling to estimate surface air temperature in Japan. *J. Geophys. Res.,* **107**, doi:10.1029/2001JD000762.

Peng, J. B., L. T. Chen, and Q. Y. Zhang, 2006: The statistic prediction model and prediction experiment of the summer rain over China by multiple factors and multi-scale variations (in Chinese). *Chin. J. Atmos. Sci.,* **30,** 596–608.

Saha, S., and Coauthors, 2012: The NCEP Climate Forecast System version 2. *J. Climate,* **27,** 2185–2208, doi:10.1175/JCLI-D-12-00823.1.

Saji, N. H., B. N. Goswami, P. N. Vinayachandran, and T. Yamagata, 1999: A dipole mode in the tropical Indian Ocean. *Nature,* **401,** 360–363.

Stine, R. A., 1985: Bootstrap prediction intervals for regression. *J. Amer. Stat. Assoc.,* **80,** 1026–1031, doi:10.1080/01621459.1985.10478220.

Wei, F. Y., and J. Y. Huang, 2010: A study of downscaling factors of atmospheric circulations in the prediction model of summer precipitation in eastern China (in Chinese). *Chin. J. Atmos. Sci.,* **34,** 202–212.

Wu, Z., B. Wang, J. P. Li, and F.-F. Jin, 2009: An empirical seasonal prediction model of the East Asian summer monsoon using ENSO and NAO. *J. Geophys. Res.,* **114,** D18120, doi:10.1029/2009JD011733.

——, Z. Jiang, J. P. Li, S. Zhong, and L. Wang, 2012a: Possible association of the western Tibetan Plateau snow cover with the decadal to interdecadal variations of northern China heatwave frequency. *Climate Dyn.,* **39,** 2393–2402, doi:10.1007/s00382-012-1439-4.

——, J. P. Li, Z. Jiang, and T. Ma, 2012b: Modulation of the Tibetan Plateau snow cover on the ENSO teleconnections: From the East Asian summer monsoon perspective. *J. Climate,* **25,** 2481–2489, doi:10.1175/JCLI-D-11-00135.1.

Zhao, S. R., and Z. S. Song, 1999: Floods and droughts in northern China and general circulation anomalies over middle and high latitudes (in Chinese). *Plateau Meteor.,* **18,** 535–540.

Zhu, C., C.-K. Park, W.-S. Lee, and W.-T. Yun, 2008: Statistical downscaling for multi-model ensemble prediction of summer monsoon rainfall in the Asia-Pacific region using geopotential height field. *Adv. Atmos. Sci.,* **25,** 867–884, doi:10.1007/s00376-008-0867-x.

Zorita, E., and H. von Storch, 1999: The analog method as a simple statistical downscaling technique: Comparison with more complicated methods. *J. Climate,* **12,** 2474–2489, doi:10.1175/1520-0442(1999)012<2474:TAMAAS>2.0.CO;2.